

## Quantum dynamics of dissipative Kerr solitons

Kilian Seibold,<sup>\*</sup> Riccardo Rota<sup>✉</sup>, Fabrizio Minganti<sup>✉</sup>, and Vincenzo Savona<sup>✉</sup>

*Institute of Physics, Ecole Polytechnique Fédérale de Lausanne (EPFL), CH-1015, Lausanne, Switzerland*

*and Center for Quantum Science and Engineering, Ecole Polytechnique Fédérale de Lausanne (EPFL), CH-1015 Lausanne, Switzerland*



(Received 8 December 2021; revised 7 April 2022; accepted 5 May 2022; published 31 May 2022)

Dissipative Kerr solitons arising from parametric gain in ring microresonators are usually described within a classical mean-field framework. Here, we develop a quantum-mechanical model of dissipative Kerr solitons in terms of the Lindblad master equation and study the model via the truncated Wigner method, which accounts for quantum effects to leading order. We show that, within this open quantum system framework, the soliton experiences a finite coherence time due to quantum fluctuations originating from losses. Reading the results in terms of the theory of open quantum systems allows us to estimate the Liouvillian spectrum of the system. It is characterized by a set of eigenvalues with a finite imaginary part and a vanishing real part in the limit of vanishing quantum fluctuations. This feature shows that dissipative Kerr solitons are a specific class of dissipative time crystals.

DOI: [10.1103/PhysRevA.105.053530](https://doi.org/10.1103/PhysRevA.105.053530)

### I. INTRODUCTION

Kerr frequency combs (KFCs) [1–6] are optical frequency combs generated by driving high- $Q$  Kerr nonlinear optical microresonators with a single-frequency continuous-wave laser [7,8]. By driving sufficiently above a power threshold determined by the Kerr nonlinearity and under appropriate conditions for the dispersion of the microresonator optical modes, the parametric process generates a comb of evenly spaced peaks in the frequency spectrum [9,10]. Since the first demonstration of KFCs [7], they have been observed countless times in a variety of platforms, materials, and spectral ranges, including silica microtoroid resonators [11,12], crystalline microresonators [13], silicon nitride waveguide resonators [14–18], diamond [19], aluminum nitride [20,21], lithium niobate [22,23], and silicon [24].

KFCs emerge from multiple parametric resonant four-wave mixing processes. On the one hand, they result from a double-balance process, in which the nonlinear frequency shifts are balanced by the mode-frequency dispersion in the microresonator. On the other hand, the cavity losses are balanced by the gain induced by the continuous-wave driving field.

For sufficiently strong drive, the frequency spacing in the comb can be as small as the free spectral range of the microresonator. In this case, a bright pulse circulating within the resonator, called the dissipative Kerr soliton (DKS), is formed [1,10,25–29]. DKSs are time-periodic solutions of an otherwise time-independent open quantum system dynamics [6,30,31]. A notable feature of DKSs is that they are dynamically stable within a classical-field approach: their wave form retains its shape *indefinitely*, making DKSs a promising resource for precision measurements [6,8], time keeping [32,33], frequency metrology [34–37], pulse shaping [15], communication engineering [38–40], high-resolution spectroscopy [41–48], and quantum information processing [49].

The rapid development of miniaturized integrated systems for KFCs and DKSs, operating at low power where quantum effects are expected to be relevant, calls for a detailed study of the influence of quantum fluctuations on the spectral and dynamical properties of DKSs in the low-power regime. While the quantum properties of KFCs have been extensively investigated [2,49–55], only recently have the quantum-mechanical properties of the DKS regime been experimentally addressed [56]. In addition, both in the case of KFCs operated below the parametric oscillation threshold and for DKSs, quantum effects have been modeled under the assumption of linearized quantum fluctuations, resulting in Gaussian quantum fields [2,49–57].

Here, we describe the quantum dynamics of DKSs using a Lindblad master equation and investigate their properties via the truncated Wigner approximation [58–63]—an approximation to model driven-dissipative quantum systems in terms of stochastic *Langevin trajectories* sampled from the Wigner quasiprobability distribution. The truncated Wigner approximation reliably describes small quantum fluctuations, which are due to the presence of nonlinearity and to the influence of the environment. These quantum fluctuations introduce mainly spatiotemporal dephasing of the DKS among different Langevin trajectories, as shown by our numerical simulations. When we model the density operator of the system, which describes the system properties averaged over the statistical ensemble of Langevin trajectories, for any finite value of the input power, the DKS does not persist indefinitely, but rather decays over time *on average*. We call the timescale over which the soliton decays on average the *soliton coherence time*. At times longer than the soliton coherence time, the average dynamics is described by a nonequilibrium steady state that restores the time-invariant symmetry of the system. We demonstrate that the soliton coherence time varies as a power law of the strength of the nonlinearity, and the semiclassical, dynamically stable DKS emerges from the average dynamics in the limit of vanishing nonlinearity and infinite driving-field amplitude.

<sup>\*</sup>kilian.seibold@epfl.ch

These results allow us to describe the DKS as an open quantum system. The theory of open quantum systems shows that, for any finite driving field and nonlinearity, the system must reach a translationally invariant steady state [64–66]. The decay of the DKS on average is a manifestation of the approach to this steady state. We demonstrate that the soliton coherence time corresponds to the so-called Liouvillian gap, i.e., the slowest timescale in the system.

Following the definition of Ref. [67], we can interpret the emergence of a DKS as a specific manifestation of a dissipative time crystal (DTC).<sup>1</sup> DTCs [67,70–89] are a peculiar phase of a driven-dissipative quantum system in which the time-translational symmetry of the equation of motion is broken and nonstationary long-lived states spontaneously occur [90]. In recent years, intense research has been devoted to investigating the conditions under which dissipation can prevent a quantum many-body system from reaching a stationary state [84,85,90,91]. This has led to numerous proposals of quantum systems supporting a DTC phase [67,73,76,84,92–99]. DTCs admit a natural explanation in terms of the eigenvalues of the Liouvillian superoperator, which generates the time evolution of the density matrix of an open quantum system [67,100]. In a DTC, multiple eigenvalues of the Liouvillian exist with vanishing real and finite imaginary parts [64,101,102], giving rise to a nonstationary dynamics with diverging relaxation time towards a steady state. The present result thus establishes a link between the long-lived DKS and the DTC phenomenon. More specifically, the Liouvillian is characterized by a set of eigenvalues whose imaginary parts are integer multiples of the frequency defining the free spectral range of the microresonator and whose real part goes to zero in the thermodynamic limit of an infinite photon number and vanishing nonlinearity.

This work is organized as follows. In Sec. II, we survey the theoretical framework used for the quantum analysis of DKSs. In Sec. III, we discuss the result obtained for the dynamics of the system: in particular, we compute the Liouvillian gap for decreasing drive power and depict a schematic representation of the spectrum of the Liouvillian. The main findings and conclusions of this work are drawn in Sec. IV.

## II. THEORETICAL FRAMEWORK

### A. The open quantum system model and Liouvillian gap

We consider a driven high- $Q$  continuous optical ring microresonator, whose schematic is shown in Fig. 1. The system Hamiltonian, in a frame rotating at the driving frequency,

<sup>1</sup>In this work, DTC stands for dissipative time crystal and not for discrete time crystal [68]. In the context of open quantum systems, time crystals have been defined in several slightly different ways. Here, we follow the definition of DTCs given in Ref. [67], where DTCs are a critical phenomenon, emerging in the thermodynamic limit, where an otherwise time-translational invariant system develops everlasting oscillations. In discrete time crystals, on the other hand, the discrete time-translation symmetry is broken in a periodically driven system. A recent experimental demonstration of the realization of a discrete time crystal in a simple, all-optical setup constituted one resonator [69].

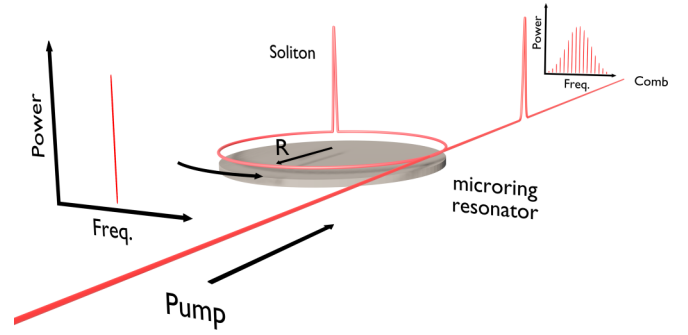


FIG. 1. Schematic representation of the generation of a Kerr optical frequency comb using a high- $Q$  Kerr optical ring microresonator. A continuous-wave source drives the ring, which induces the propagation of a soliton (depicted in red) along the ring. The output signal shows the optical frequency comb. When all the resonator modes participate in the parametric process, the nonlinear dynamics give rise to a DKS.

reads ( $\hbar = 1$ )

$$\hat{\mathcal{H}} = \sum_l \sigma_l \hat{a}_l^\dagger \hat{a}_l + \frac{\kappa}{2} F (\hat{a}_0^\dagger + \hat{a}_0) + \frac{g}{2} \sum_{m,n,p,q} \delta_{m+p,n+q} \hat{a}_n^\dagger \hat{a}_q^\dagger \hat{a}_m \hat{a}_p, \quad (1)$$

where  $\hat{a}_l$  ( $\hat{a}_l^\dagger$ ) is the annihilation (creation) operator of the  $l$ th angular momentum mode (i.e., the discrete set of whispering gallery modes), satisfying the commutation relation  $[\hat{a}_j, \hat{a}_k^\dagger] = \delta_{jk}$ . Only the lowest-energy mode of the microresonator ( $l = 0$ ) is driven by an external continuous-wave laser of amplitude  $F$ . The Kerr interaction strength can be obtained from a microscopic model as  $g = \hbar \omega_0^2 c n_2 / (n_0^2 A_{\text{eff}} L)$  [57,103,104], where  $c$  is the speed of light in vacuum,  $n_0$  is the refractive index of the medium at the fundamental resonator frequency  $\omega_0$ ,  $n_2$  is the Kerr parameter,  $A_{\text{eff}}$  is the effective mode area, and  $L$  is the resonator length. Note that miniaturizing the resonator means decreasing the effective mode volume ( $V_{\text{eff}} = A_{\text{eff}} L$ ) and hence increasing the Kerr interaction strength  $g$ . We set  $\sigma_l = \sigma_0 + \omega_0 - \omega_l$ , where  $\sigma_0 = \omega_p - \omega_0$  is the detuning between the driving frequency  $\omega_p$  and the fundamental resonator frequency  $\omega_0$  and  $\omega_l$  is the dispersion relation (which in this work is assumed to be parabolic,  $\omega_l \propto l^2$ ; see also Fig. 2).

In order to account for the finite lifetime of the photons inside the microresonator, we describe the dynamics of the open system in terms of its reduced density matrix  $\hat{\rho}$ . Assuming a weakly interacting and memoryless environment (i.e., Born and Markov approximations),  $\hat{\rho}$  solves the Lindblad quantum master equation [58,105]:

$$\frac{d\hat{\rho}}{dt} = \mathcal{L}\hat{\rho} = -i[\hat{\mathcal{H}}, \hat{\rho}] + \kappa \sum_l \mathcal{D}[\hat{a}_l] \hat{\rho}. \quad (2)$$

Here,  $\mathcal{D}[\hat{a}_l] \hat{\rho} = \hat{a}_l \hat{\rho} \hat{a}_l^\dagger - 1/2(\hat{a}_l^\dagger \hat{a}_l \hat{\rho} + \hat{\rho} \hat{a}_l^\dagger \hat{a}_l)$  is the dissipator in Lindblad form accounting for the loss of photons from a mode  $l$  into the environment, and  $\kappa$  is the dissipation rate (which we assume is uniform).  $\mathcal{L}$  is the Liouvillian superoperator, and its spectrum, defined by the equation  $\mathcal{L}\hat{\rho}_j = \lambda_j \hat{\rho}_j$ , encodes the full dynamics of an open quantum system. In most

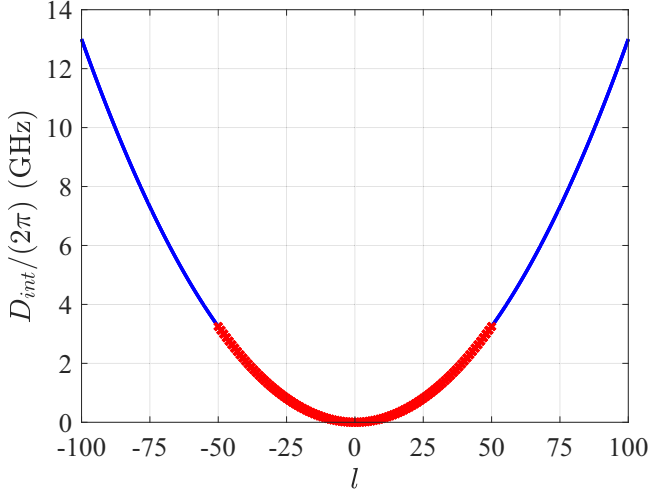


FIG. 2. Integrated dispersion relation  $D_{\text{int}}(l)$  versus relative mode number  $l$ . The red markers show the 101 spectral modes that are considered in the numerical simulations. The parameters are given in the text and correspond to typical experimental situations [18].

physically relevant cases, the Liouvillian superoperator  $\mathcal{L}$  has a unique zero eigenvalue, which defines the nonequilibrium steady state  $d\hat{\rho}_{\text{ss}}/dt = 0$  [65,66]. All other eigenvalues of the Liouvillian have a negative real part, determining the irreversible dissipative dynamics towards the steady state. The eigenvalue  $\lambda_j$ , whose real part is the smallest nonzero in modulus, defines the Liouvillian gap  $\Lambda$ .  $\Lambda$  corresponds to the inverse of the longest relaxation timescale of the system. Critical phenomena, such as dissipative phase transitions and the emergence of DTCs, are associated with a closure of the Liouvillian gap, i.e.,  $\Lambda \rightarrow 0$ . A complete account of the spectral theory of Liouvillians can be found in, e.g., Ref. [66].

### B. Classical-field approach to solitons

To numerically simulate the optical ring microresonator, we will consider a finite number of modes  $N_m$  around the  $l = 0$  driven mode. Except when otherwise specified, we will set  $N_m = 101$  (i.e., we consider only the modes  $l = [-50, -49, \dots, 50]$ ). We verified that the results shown hereafter are affected in only one part in  $10^5$  on the total population as a result of this truncation in the number of modes. Despite this simplification, the numerically exact solution of the master equation (2), in the regime of large occupation considered here, would be computationally unfeasible.

DKSs in the weakly nonlinear regime are usually modeled in terms of the classical Gross-Pitaevskii (GP) equation, in which the classical-field amplitudes of the resonator modes  $\alpha_l = \langle \hat{a}_l \rangle$  obey the equation

$$\begin{aligned} \alpha_l(t + dt) = & \alpha_l(t) + i \left\{ \left( \sigma_l + i \frac{\kappa}{2} \right) \alpha_l(t) \right. \\ & \left. + g \sum_{m,n,p} \delta_{n+l,m+p} \alpha_m(t) \bar{\alpha}_n(t) \alpha_p(t) - \frac{\kappa}{2} F \delta_{l,0} \right\} dt, \end{aligned} \quad (3)$$

where  $\bar{\alpha}_n$  indicates the complex conjugate of the field  $\alpha_n$ . The GP equation leads directly to the *Lugiato-Lefever equation* [106,107] describing the real-space dynamics of the soliton.<sup>2</sup>

Note that Eq. (3) is invariant under the scaling relation

$$\tilde{\alpha}_l = \alpha_l / \sqrt{\tilde{N}}, \quad \tilde{g} = g \tilde{N}, \quad \tilde{F} = F / \sqrt{\tilde{N}}, \quad (4)$$

where we introduced the dimensionless scaling parameter  $\tilde{N}$ . The GP solution for the rescaled field  $\tilde{\alpha}_l$  depends on only the product  $\tilde{F}^2 \tilde{g} = F^2 g$ . In what follows, all results are obtained by setting  $\tilde{F}^2 \tilde{g} = 1$ , which corresponds to a case well above the threshold for soliton formation (see discussion in Sec. III A).

### C. The truncated Wigner approximation

Theoretical studies of DKSs beyond the GP approximation have been mostly carried out by assuming linearized quantum fluctuations around the GP solution, i.e., Gaussian quantum fields [2,49–57]. Quantum-mechanical properties of the ring resonator can be better described with methods based on quasiprobability distributions [58,59], such as the truncated Wigner approximation (TWA). Indeed, in cases where the quantum effects are a small (but non-negligible) correction to the classical limit of very large photon occupation, these methods account also for non-Gaussian quantum fluctuations, which become relevant when increasing  $g$ . Below, we recall the main ideas behind the TWA; for a more detailed derivation, we refer the interested reader to Refs. [58–63].

For a single mode of the electromagnetic field, the Wigner quasiprobability distribution function  $W(\alpha)$  of a given quantum state expresses the quasiprobability distribution function in the phase space spanned by  $Q$  and  $P$ , with  $\alpha = (Q + iP)/\sqrt{2}$ . The quantities  $Q$  and  $P$  are the (real) eigenvalues of the electromagnetic field quadratures  $\hat{q}$  and  $\hat{p}$ , with  $\hat{a} = (\hat{q} + i\hat{p})/\sqrt{2}$ . For  $N_m$  modes, the Wigner function  $W(\vec{\alpha})$  is easily generalized in terms of  $N_m$  complex fields  $\vec{\alpha} = \{\alpha_{-N_m/2}, \dots, \alpha_{N_m/2}\}$ . The density matrix can be expressed in terms of the Wigner function as [109]

$$W(\vec{\alpha}) = \left( \frac{2}{\pi} \right)^{N_m} \text{Tr} \left[ \prod_{l=-N_m/2}^{N_m/2} \hat{D}(\alpha_l) e^{i\pi \hat{a}_l^\dagger \hat{a}_l} \hat{D}(-\alpha_l) \hat{\rho} \right], \quad (5)$$

where  $\hat{D}(\alpha_l) = \exp(\alpha_l \hat{a}_l^\dagger - \alpha_l^* \hat{a}_l)$  is the displacement operator.  $W(\vec{\alpha})$  is a quasiprobability because it is real valued, but it can take negative values. The Lindblad master equation for the density matrix of a quantum optical system characterized by a Kerr nonlinearity maps onto a third-order differential equation for  $W(\vec{\alpha})$  in the variables  $\vec{\alpha}$ . The exact solution of this equation is as cumbersome as the solution of the corresponding master equation. However, when in the presence of a small Kerr nonlinearity  $g$  and for sufficiently well-behaved functions, the third-order terms can be neglected, resulting

<sup>2</sup>Usually, the GP (Lugiato-Lefever) equations are written as a set of coupled ordinary differential equations. Here, we represent them as a set of differential forms in order to be consistent with Eq. (6), which contains the stochastic term  $\chi_{i,\mu}(t)$ . Otherwise, its definition would require us to introduce stochastic integration. We refer the interested reader to Ref. [108].

in the TWA [60,62]. The TWA correctly describes quantum fluctuations up to the lowest (i.e., second) order in  $\hbar$  with respect to the mean-field equation, holding in the limit of very large photon occupation [63].

The advantage of the TWA is that it defines a Fokker-Planck equation for the complex fields  $\bar{\alpha}$ . By choosing an appropriate initial distribution, the Fokker-Planck equation for  $W(\bar{\alpha})$  can be cast into a set of Langevin equations for the corresponding stochastic processes in the complex fields  $\alpha_{l,\mu}(t)$ . Each instance of the stochastic process thus results in a Langevin trajectory, and the average solutions of the Fokker-Planck and master equations are obtained from averaging over the statistical ensemble of possible trajectories. In the case of the DKS model considered here, the Langevin equations read

$$\begin{aligned} \alpha_{l,\mu}(t+dt) = & \alpha_{l,\mu}(t) + i \left\{ \left( \sigma_l + i \frac{\kappa}{2} - g \right) \alpha_{l,\mu}(t) \right. \\ & + g \sum_{m,n,p} \delta_{n+l,m+p} \alpha_{m,\mu}(t) \bar{\alpha}_{n,\mu}(t) \alpha_{p,\mu}(t) \\ & \left. - \frac{\kappa}{2} F \delta_{l,0} \right\} dt + \sqrt{\kappa dt/2} \chi_{l,\mu}(t). \end{aligned} \quad (6)$$

Here, the index  $\mu$  runs on distinct Langevin trajectories, and the term  $\chi_{l,\mu}(t)$  is a complex Gaussian stochastic variable defining each specific trajectory and is characterized by correlation functions  $\langle \chi_l(t) \chi_l(t') \rangle = 0$  and  $\langle \chi_l(t) \bar{\chi}_{l'}(t') \rangle = dt \delta_{l,l'} \delta(t-t')$ . The noise terms  $\chi_{l,\mu}(t)$  therefore account for the quantum fluctuations induced by photon losses.

Within the TWA, it is possible to obtain the expectation value of the symmetrized product of operators in terms of an average over the sampled Langevin trajectories, according to the formula

$$\text{Tr}[\hat{\rho}(t) \{ (\hat{a}_j^\dagger)^n, (\hat{a}_k)^m \}_{\text{sym}}] = \langle [\bar{\alpha}_j(t)]^n [\alpha_k(t)]^m \rangle_{\text{stoch}}, \quad (7)$$

where we use the notation for the stochastic average  $\langle \alpha_j(t) \rangle_{\text{stoch}} = [\sum_{\mu=1}^{N_{\text{traj}}} \alpha_{j,\mu}(t)] / N_{\text{traj}}$ . In other words, the expectation value of any observable is obtained by sampling a sufficiently large number  $N_{\text{traj}}$  of Langevin trajectories, thus recovering the results of the Fokker-Planck equation associated with the TWA. In the following, the convergence of the results with respect to the number of considered trajectories  $N_{\text{traj}}$  used for the averaging is carefully checked.

From the solutions of the Langevin equations, the number of photons in each mode  $l$  of the microresonator is expressed by

$$N_l(t) = \langle |\alpha_l(t)|^2 \rangle_{\text{stoch}} - \frac{1}{2}, \quad (8)$$

and the photon density at position  $\theta$  is obtained as

$$N_\theta(t) = \langle |\psi_\mu(\theta, t)|^2 \rangle_{\text{stoch}} - \frac{N_m}{4\pi}, \quad (9)$$

where

$$\psi_\mu(\theta, t) = \frac{1}{\sqrt{2\pi}} \sum_l e^{i\theta l} \alpha_{l,\mu}(t). \quad (10)$$

Notice that Eqs. (8) and (9) clearly illustrate how quantum fluctuations are approximately described by the TWA. In particular, Eq. (8) shows that the classical field modeled by the Langevin equation contains quantum fluctuations corresponding to half a photon per mode. Similarly, Eq. (9) suggests

that the Langevin field a discrete element of real space  $\Delta\theta$ , defined by the momentum cutoff introduced by truncating to  $m$  modes, contains quantum fluctuations corresponding to  $N_m/4\pi$  photons.

In contrast to the GP equation, Eq. (6) is not invariant under the rescaling introduced in Eq. (4). Indeed, applying the same rescaling to Eq. (6), one obtains

$$\begin{aligned} \tilde{\alpha}_{l,\mu}(t+dt) = & \tilde{\alpha}_{l,\mu}(t) + i \left\{ \left( \sigma_l + i \frac{\kappa}{2} - \frac{\tilde{g}}{\tilde{N}} \right) \tilde{\alpha}_{l,\mu}(t) \right. \\ & + \tilde{g} \sum_{m,n,p} \delta_{n+l,m+p} \tilde{\alpha}_{m,\mu}(t) \tilde{\alpha}_{n,\mu}(t) \tilde{\alpha}_{p,\mu}(t) \\ & \left. - \frac{\kappa}{2} \tilde{F} \delta_{l,0} \right\} dt + \sqrt{\kappa dt / (2\tilde{N})} \tilde{\chi}_{l,\mu}(t), \end{aligned} \quad (11)$$

which explicitly depends on  $\tilde{N}$ .

For coherent states, the scaling parameter  $\tilde{N}$  is proportional to the ratio between the field intensity and the fluctuations of the field quadratures and therefore can be interpreted as a measure of the *classicality* of the optical system. Small values of  $\tilde{N}$  describe a regime with sizable quantum effects, where quantum fluctuations are of the same order as the field intensity. As  $\tilde{N}$  increases, fluctuations become smaller compared to the field intensity, and quantum effects become less relevant. This interpretation of the quantity  $\tilde{N}$  holds also in the TWA, which describes quantum states beyond the coherent-state approximation. Indeed, for large values of  $\tilde{N}$ , Eq. (11) approaches the GP equation (3). Our goal is to investigate how the quantum effects influence the dynamics of a DKS by comparing the solution of Eq. (11) obtained for different values of  $\tilde{N}$  while keeping all the other parameters unchanged. Notice that, in light of the scaling relations in Eq. (4), this procedure corresponds to solving the Lindblad master equation (2) for different values of the nonlinearity  $g$  and the pump amplitude  $F$  in such a way that the product  $F^2 g$  remains constant.

### III. RESULTS

#### A. Regime of parameters

A microring resonator is characterized by its radius  $R$  (and length  $L = 2\pi R$ ), cross section  $A_{\text{eff}}$ , quality factor  $Q$ , resonant central frequency  $f_0 = \omega_0/2\pi$ , refractive index  $n_0$ , the Kerr parameter  $n_2$ , and the group velocity dispersion  $\beta_2$ . The system is driven by a laser with frequency  $\omega_p$ .

From these quantities, the loss rate  $\kappa$  and the nonlinearity  $g$  in the Lindblad master equation (2) can be determined, respectively, as [57,103,104]

$$\kappa = \frac{\omega_0}{Q}, \quad (12)$$

$$g = \frac{\hbar \omega_0^2 c n_2}{n_0^2 A_{\text{eff}} L}, \quad (13)$$

where  $c$  is the speed of light. Close to the driving-field frequency (i.e.,  $\omega_0 \simeq \omega_p$ ), the mode dispersion of the microresonator is approximated using a second-order polynomial,

$$\omega_l = \omega_0 + D_1 l + \frac{1}{2} D_2 l^2, \quad (14)$$

where  $D_1 = c/(n_0 R)$  is the mean free spectral range and  $D_2 = -(c/n_0) D_1^2 \beta_2$ . A positive value of  $D_2$  characterizes the

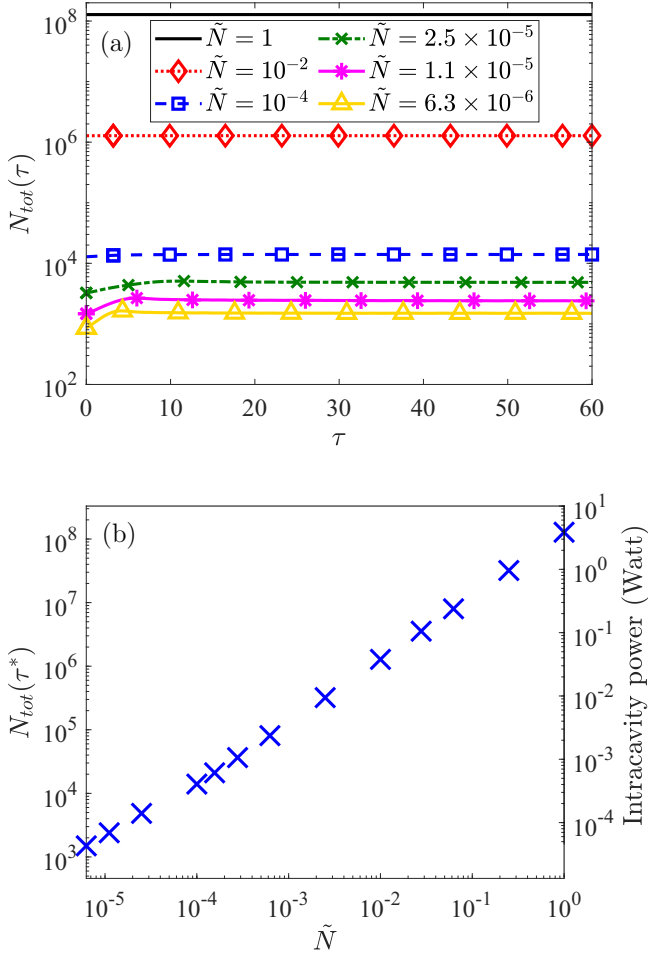


FIG. 3. (a) Time evolution of the total number of photons in the ring for different values of  $\tilde{N}$ . (b) Total number of photons in the ring and intracavity power versus the scaling parameter  $\tilde{N}$ . The values are taken at  $\tau^* = 60$ , where the photon number reached a stationary distribution.

anomalous dispersion regime, which is needed for the formation of DKSs [18]. The integrated dispersion relation  $D_{int}(l)$  relative to the driving mode at  $l = 0$  is defined by (see Fig. 2)

$$D_{int}(l) \equiv \omega_l - (\omega_0 + D_1 l). \quad (15)$$

The driving parameter  $F$  is related to the power of the external driving field through the relation  $P_{ext} = \hbar \omega_p \kappa F^2 / (4\eta)$ , where  $\eta$  is the coupling efficiency (we assume critical coupling, i.e.,  $\eta = 1/2$ ).

Typical parameters for a silicon nitride ( $\text{Si}_3\text{N}_4$ ) ring resonator encapsulated in silica [18,110], with  $R = 100 \mu\text{m}$ , are  $A_{eff} = 0.73 \times 2.5 \times 10^{-12} \text{ m}^2$  [110];  $Q = 1.5 \times 10^6$  [18];  $f_0 = \omega_0/2\pi = 193.5 \text{ THz}$  [111], corresponding to a wavelength  $\lambda = 1.55 \mu\text{m}$  in the telecom range;  $n_0 = 1.99$ ; and  $n_2 = 2.4 \times 10^{-19} \text{ m}^2/\text{W}$  [112]. Consequently, following Eqs. (12) and (13),  $\kappa/2\pi = 1.3 \times 10^8 \text{ Hz}$ , and  $g/2\pi = 0.39 \text{ Hz} = 0.49 \times 10^{-9} \kappa$ .

Necessary conditions on the driving-field detuning and intensity must be fulfilled in order to observe a DKS in the solution of the GP equation. In particular, we set the driving-field frequency to  $\omega_p/2\pi = 193.47 \text{ THz}$ , i.e., a detun-

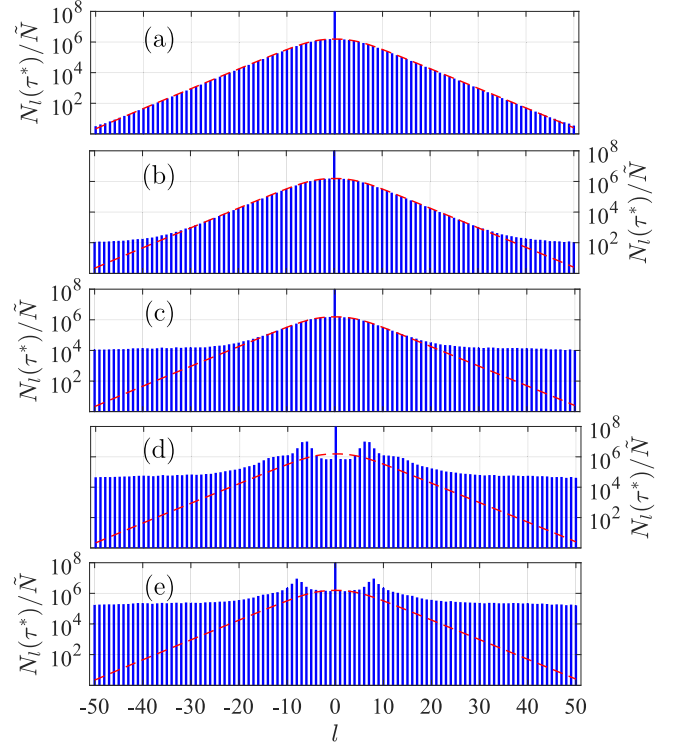


FIG. 4. Snapshot of the mode occupation at  $\tau^*$  for (a)  $\tilde{N} = 1$ , (b)  $10^{-2}$ , (c)  $10^{-4}$ , (d)  $2.5 \times 10^{-5}$ , and (e)  $6.3 \times 10^{-6}$ . The red dashed lines show the GPE prediction for the mode occupation. Parameter values are  $\sigma_0 = -1.024\kappa$ ,  $D_1 = 1.8587 \times 10^3 \kappa$ ,  $D_2 = 2.02 \times 10^{-2} \kappa$ ,  $g/2\pi = 0.49 \times 10^{-9} \kappa$ , and  $F = 1.8 \times 10^4$ .

ing  $\sigma_0/2\pi = -0.132 \text{ GHz}$  [18]. The driving-field amplitude  $F$  must be larger than a minimum threshold value  $F_{thr}$  [26,57,107]. Expressing the minimum threshold condition in terms of the parameters of the present model results in  $F_{thr}^2 g/\kappa = \tilde{F}_{thr}^2 \tilde{g}/\kappa = 1/2$ . Given the values of  $\kappa$  and  $g$  introduced above, the minimum threshold is  $\tilde{F}_{thr} = 0.9 \times 10^4$ . Here, to ensure the appearance of the DKS within the GP equation [107], we set in all the analysis that follows  $F = 1.8 \times 10^4$ , i.e., twice the minimum threshold, corresponding to a laser power  $P_{ext} = 1.7 \times 10^{-2} \text{ W}$  (similar to that used in Ref. [18]). This value and the value chosen for  $g$  therefore correspond to the typical regime of current experiments, like those in Refs. [18,110], where quantum fluctuations are very small relative to the classical field. We arbitrarily set  $\tilde{N} = 1$  for this choice of  $F$  and  $g$ . In what follows, we will study the results of the TWA for values of  $\tilde{N}$  ranging between  $\tilde{N} = 6.3 \times 10^{-6}$  and  $\tilde{N} = 1$ . Values of  $\tilde{N} < 1$  describe cases with larger nonlinearity  $\tilde{g}$  and smaller driving-field amplitude  $\tilde{F}$  than the values of  $F$  and  $g$  quoted above, for which quantum effects are larger. Finally, we define the dimensionless time parameter  $\tau = \kappa t/2$ .

## B. Dynamics of the soliton

We study the time evolution of DKSs by numerically solving Eq. (11) for the rescaled fields  $\tilde{\alpha}_l$  obtained using the TWA approach. Equation (11) gives rise to a stochastic trajectory in the space of the fields  $\tilde{\alpha}_l$ , determined by the specific real-

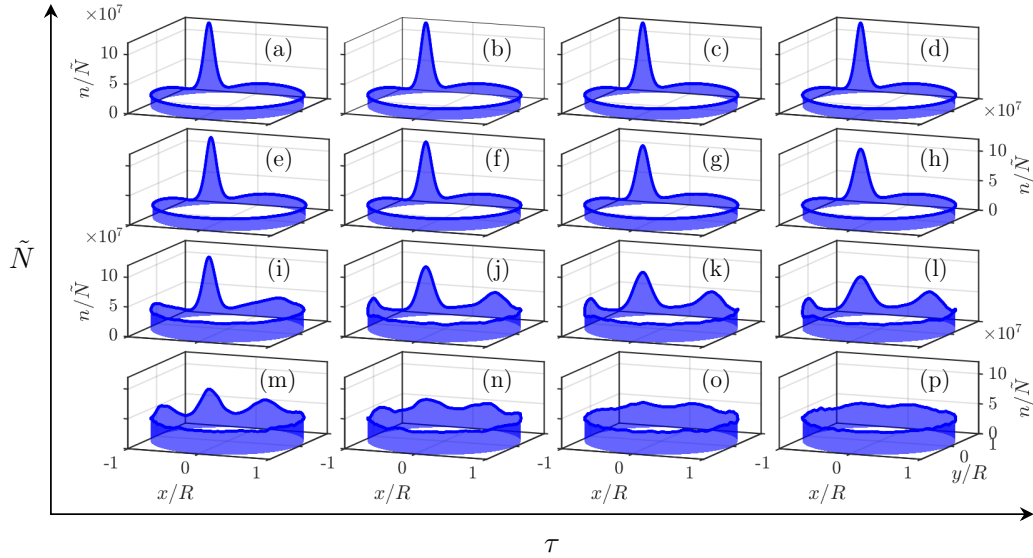


FIG. 5. Snapshot of the field density in real space at (a), (e), (i), and (m)  $\tau = 0.5 \times 10^4 \kappa/2T \approx 8.5$ , (b), (f), (j), and (n)  $\tau = 1.5 \times 10^4 \kappa/2T \approx 25.4$ , (c), (g), (k), and (o)  $\tau = 2.5 \times 10^4 \kappa/2T \approx 42.3$ , and (d), (h), (l), and (p)  $\tau = 3.5 \times 10^4 \kappa/2T \approx 59.2$ , for (a)–(d)  $\tilde{N} = 10^{-2}$ , (e)–(h)  $10^{-4}$ , (i)–(l)  $2.5 \times 10^{-5}$ , and (m)–(p)  $6.3 \times 10^{-6}$ . The density is plotted as a function of the coordinates  $x = R \cos(\theta)$  and  $y = R \sin(\theta)$ , with  $R$  being the radius of the ring resonator. The soliton is depicted at a time multiple of  $T = 2\pi/D_1 \approx 4.2 \times 10^{-12}$  s; the rotation period of the soliton is along the ring. For this choice of time, the peak of the soliton always occupies the same position in the ring, allowing an easier comparison between the different plots.

ization of the noise term  $\chi_{l,\mu}(t)$ . All results in what follows are obtained by averaging over several trajectories arising from different realizations of  $\chi_{l,\mu}(t)$ . As initial conditions, we assume each mode is in a coherent state corresponding to the solution  $\tilde{\alpha}_l^{\text{GPE}}$  of the GP equation, which in turn is obtained by numerically integrating Eq. (3) at long times. This choice has the advantage of avoiding the integration of a possibly long transient before the actual formation of a soliton within a single trajectory. In the TWA formalism, this choice of initial condition implies that the initial condition  $\tilde{\alpha}_l(t=0)$  in Eq. (11) must be sampled from a Gaussian distribution of variance  $1/(2\tilde{N})$  and average  $\tilde{\alpha}_l^{\text{GPE}}$ .

More precisely, we set

$$\tilde{\alpha}_{l,\mu}(t=0) = \tilde{\alpha}_l^{\text{GPE}} + \frac{1}{\sqrt{2\tilde{N}}} \eta_{l,\mu}, \quad (16)$$

where  $\eta_{l,\mu}$  is a complex random variable of zero mean, verifying  $\langle \eta_{l,\mu} \eta_{l,\mu'} \rangle = 0$  and  $\langle \bar{\eta}_{l,\mu} \eta_{l,\mu'} \rangle = \delta_{\mu,\mu'}$ .

Figure 3(a) displays the total number of photons in the ring  $N_{\text{tot}}$  vs time for varying  $\tilde{N}$ . The small initial transient is due to the difference between the solution of the GP equation, which was used as the initial condition, and the actual TWA solution. In what follows, in the analysis of the spectral features of the DKS, data will be taken in the vicinity of  $\tau^* = 60$ , a time sufficiently long for the rapidly decaying transient effects to play no role. In Fig. 3(b) the dependence of  $N_{\text{tot}}(\tau^*)$  on  $\tilde{N}$  is shown to be linear,  $N_{\text{tot}} \sim \tilde{N}$ . Thus, the intracavity power  $P_l = \hbar\omega_p D_1 N_{\text{tot}}/(2\pi)$  (which is proportional to the total number of photons in the microring) also depends linearly on  $\tilde{N}$ . We conclude that a small photon occupation and low intracavity power are reached only for small  $\tilde{N}$ .

In Fig. 4, the photon number in the  $l$ th mode  $N_l(\tau^*)$  [see Eq. (8)] is displayed for different values of  $\tilde{N}$ . For the largest value of  $\tilde{N}$ , the output field is in agreement with the predic-

tion of the GP equation, while smaller values of  $\tilde{N}$  gradually display increasing features of quantum fluctuations.

In Fig. 5 the photon density along the ring  $n(\theta, \tau) = N_\theta(\tau)/(2\pi)$ , with  $N_\theta$  being the number of photons in position  $\theta$  [see Eq. (9)], is displayed at increasing times  $\tau$  (left to right) and for increasing  $\tilde{N}$  (bottom to top).<sup>3</sup> For  $\tilde{N} = 1$  in Figs. 5(a)–5(d), the soliton displays a constant profile within the considered time window. However, for smaller  $\tilde{N}$ , i.e., increasing the relevance of quantum fluctuations, the soliton profile changes in time, in particular by showing a decreasing contrast of the intensity profile along the ring. For the smallest value  $\tilde{N} = 6.3 \times 10^{-6}$  [Figs. 5(m)–5(p)], the photon density quickly approaches a uniform distribution over the ring. We conclude that the soliton is gradually smeared out over time by quantum fluctuations, and smaller values of  $\tilde{N}$  correspond to faster disappearance of the soliton.

Single Langevin trajectories, from which TWA results are drawn, give insight into the process leading to the disappearance of the soliton in Fig. 5 as a result of quantum fluctuations. A trajectory represents, in the limit of small nonlinearities, the possible outcome of an experiment with homodyne measurement of the output field [113]. In Fig. 6, we plot three trajectories at different values of  $\tilde{N}$  and at two different times. For  $\tilde{N} = 10^{-2}$  a sharp soliton peak in the photon density persists at both short and long times. The position and height of the peak slightly vary with the sampled noise realization, but this difference is negligible with respect to the GP solution. At the intermediate value  $\tilde{N} = 10^{-4}$ , a similar behavior appears only at shorter times, while at longer times the trajectories differ significantly. For the smallest value  $\tilde{N} = 4.4 \times 10^{-5}$

<sup>3</sup>Notice that this definition ensures that  $N_{\text{tot}}(\tau) = \sum_l N_l(\tau) = \int d\theta n(\theta, \tau)$ .

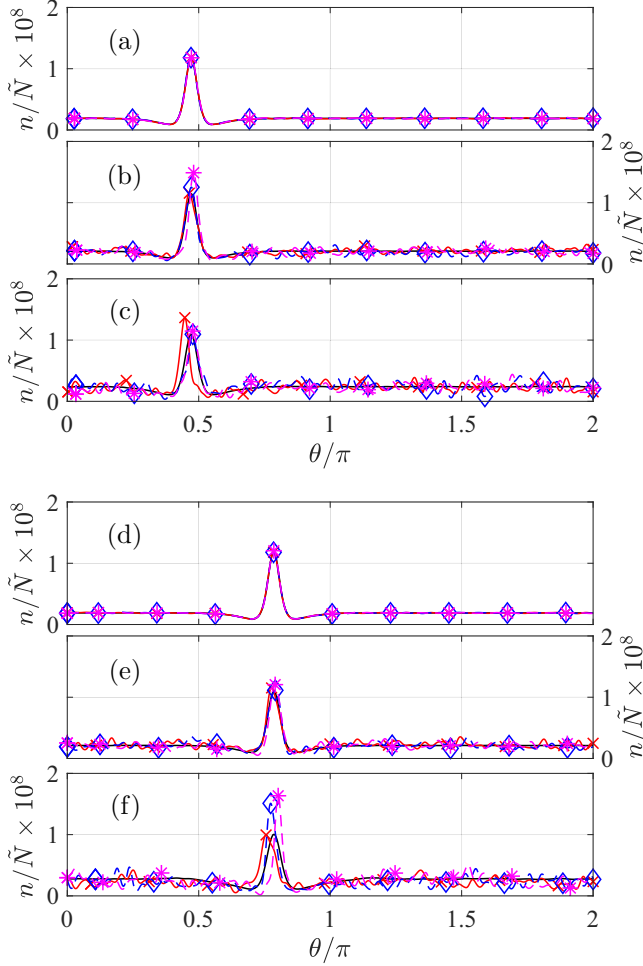


FIG. 6. Occupation density in real space for (a) and (d)  $\tilde{N} = 10^{-2}$ , (b) and (e)  $10^{-4}$ , and (c) and (f)  $4.4 \times 10^{-5}$  at (a)–(c)  $\tau = 6$  and (d)–(f)  $\tau = 15$ . Solid lines are averages over  $10^4$  trajectories, while three single trajectories are plotted as crosses, stars, and diamonds.

considered, we observe a faster loss of coherence between different trajectories. Since the effect increases when the non-linearity is larger, we conclude that fluctuations, which are responsible for only a small dephasing among different trajectories at short time, accumulate as time passes, leading to a loss of spatial and temporal coherence, resulting in the smearing out of the DKS once an average is taken (see Fig. 5).

From the point of view of open quantum systems, the density matrix  $\hat{\rho}(t)$ , evolving under the Lindblad master equation in Eq. (2), describes the *average* time evolution of the microring resonator. Under quite general hypotheses, an open quantum system admits a unique steady state  $\hat{\rho}_{ss}$ , towards which the system density matrix will converge. In this sense, a system which at  $t = 0$  displays a soliton will eventually converge to such a steady state. We can thus interpret the loss of soliton coherence in Fig. 5 as the decay towards the steady state and call the timescale on which this process occurs the *soliton coherence time*. Thus, to quantify the soliton coherence time, we compute the Liouvillian gap  $\Lambda$  (i.e., the slowest decay rate). Indeed, the DKS is the longest-lived process of Eq. (2), and thus,  $\Lambda$  is the inverse of soliton coherence time (see Sec. II A). To extract  $\Lambda$ , we consider the time evolution

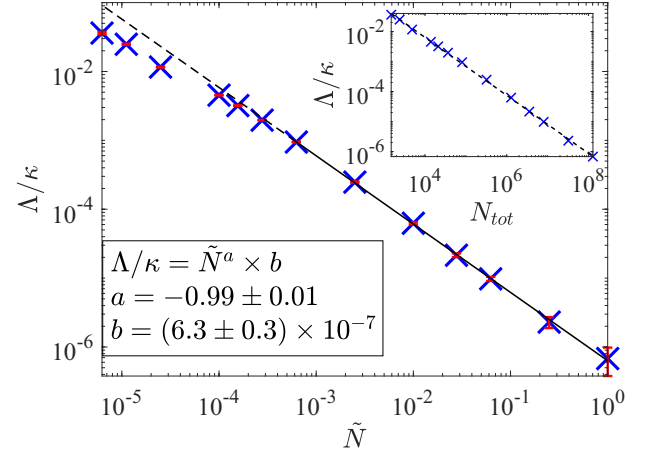


FIG. 7. (a) Liouvillian gap  $\Lambda$  versus  $\tilde{N}$ . The error bars of the fit (in red) show the standard error (the 95% confidence interval) of each point. The power-law fit of the Liouvillian gap for  $\tilde{N} \geq 6.3 \times 10^{-4}$  is shown by the solid line. The coefficients of the fit are  $\Lambda/\kappa = \tilde{N}^a \times b$ , with  $a = -0.99 \pm 0.01$  and  $b = (6.3 \pm 0.3) \times 10^{-7}$ . Inset: the Liouvillian gap versus the total number of photons inside the ring microresonator at long times (see Fig. 3). The dashed line represents a power-law fit.

of the *contrast* of the soliton defined by

$$C(\tau) = \frac{\max_{\theta} [n(\theta, \tau)]}{\int_0^{2\pi} n(\theta, \tau) d\theta / 2\pi}. \quad (17)$$

For a flat intensity profile along the ring, the value of  $C(\tau)$  approaches 1. We estimate  $\Lambda$  by assuming an exponential behavior vs time,  $C(\tau) \simeq 1 + A \exp(-\Lambda\tau)$ , and fitting the numerical results.

In Fig. 7, the Liouvillian gap is plotted as a function of  $\tilde{N}$ . For large  $\tilde{N}$  the Liouvillian gap follows a power law  $\Lambda \sim \tilde{N}^a$ , with  $a < 0$ , indicating that the gap closes in the classical limit  $\tilde{N} \rightarrow \infty$ . A similar power law emerges in the dependence of  $\Lambda$  on  $N_{tot}$  (inset of Fig. 7). Here,  $\Lambda \sim N_{tot}^{\eta}$ , with  $\eta = -0.97 \pm 0.01$ . This analysis indicates the range of values of the input power for which a finite soliton coherence time may be observed.

Summing up, the loss of coherence at the single-trajectory level appears mainly as a change in the soliton position with respect to the GP solution.<sup>4</sup> And since this effect emerges only in Langevin trajectories (stemming from the TWA) and not in the GP equation, the loss of coherence is due to quantum (i.e., beyond semiclassical) fluctuations. Quantum fluctuations have two contributions: One comes from the non-commutative nature of the Hamiltonian terms, and the other comes from the system's interaction with the environment, which induces dissipation. The truncated Wigner approximation takes them both into account (up to order  $\hbar$ ). The two additional terms accounting for these fluctuations can

<sup>4</sup>While, at the single-trajectory level, the processes of variation in amplitude and spatiotemporal position are dominant, for even smaller  $\tilde{N}$  and/or larger times, other phenomena like the appearance of multiple peaks are observed.

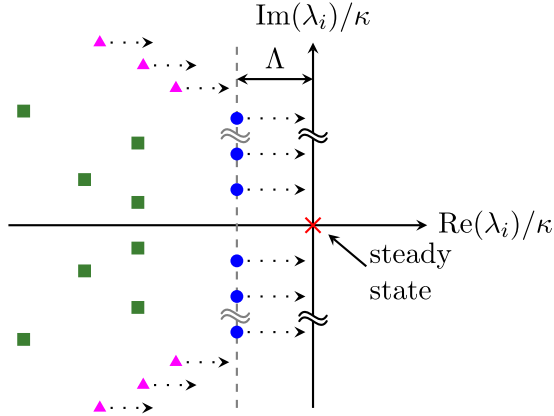


FIG. 8. Schematic representation of the spectrum of the Liouvillian. The spectrum always has one zero eigenvalue, corresponding to the steady state (red cross). A set of eigenvalues with a vanishing real part and equally spaced imaginary parts emerges in the classical limit of large  $\tilde{N}$  (blue circles). The Liouvillian gap is the distance between the complex eigenvalues with the largest real part and the imaginary axis.

be obtained by comparing Eq. (6) with Eq. (3): a term proportional to  $g$  (producing a deterministic effect with respect to the GP equation) and the noise term  $\chi_{l,\mu}$  (which induces random changes at a single trajectory and thus mixedness in the density matrix). It is the combined effects of these two terms which leads to the soliton finite coherence time.

### C. DKS as a dissipative time crystal

The occurrence of a time-crystalline phase in a dissipative system is signaled by the emergence of several eigenvalues of the Liouvillian, whose real part tends to zero in the thermodynamic limit and whose imaginary part is a multiple of a finite frequency, as schematically shown in Fig. 8.

We extract the imaginary part of the Liouvillian eigenvalues with the largest real part by studying the Fourier spectrum of the KFC,

$$S_\varphi(\omega) = \left| \frac{\sqrt{2\pi}}{N_{\mathcal{T}} T} \int_{t_0}^{t_0 + N_{\mathcal{T}} T} dt e^{i\omega t} \varphi(\theta = 0, t) \times \tilde{N} \right|^2, \quad (18)$$

where  $\varphi(\theta, t) = \text{Tr}[\hat{\rho}(t) \times 1/\sqrt{2\pi} \sum_l e^{i\theta l} \hat{a}_l]$  and  $T = 2\pi/D_1$  is the rotation period of the soliton along the ring. The parameters  $t_0 = 20\kappa^{-1}$  and  $N_{\mathcal{T}} = 2 \times 10^4$  are set to ensure that the dynamics is dominated by the eigenvalues with the largest real part. Notice that, for these parameters,  $S_\varphi(\omega)$  does not depend significantly on the position  $\theta$  at which the field  $\varphi$  is considered.

The computed power spectra are plotted in Fig. 9. From the spectra, we extract the frequency spacing  $\Omega_{\text{soliton}} = D_1 = 1.86 \times 10^3 \kappa$ , which coincides with the classical prediction, indicating that quantum fluctuations affect mainly the coherence time of the soliton while having negligible effects on the period of its motion along the ring. For the smallest value of  $\tilde{N} = 6.3 \times 10^{-6}$ , where  $\Lambda \simeq 3 \times 10^{-2} \kappa$ , the ratio  $\Lambda/\Omega_{\text{soliton}}$  is of the order of  $10^{-4}$ . These results indicate that the peculiar structure of the frequency comb (i.e., the presence of equally spaced, narrow spectral lines) is preserved even in the regime

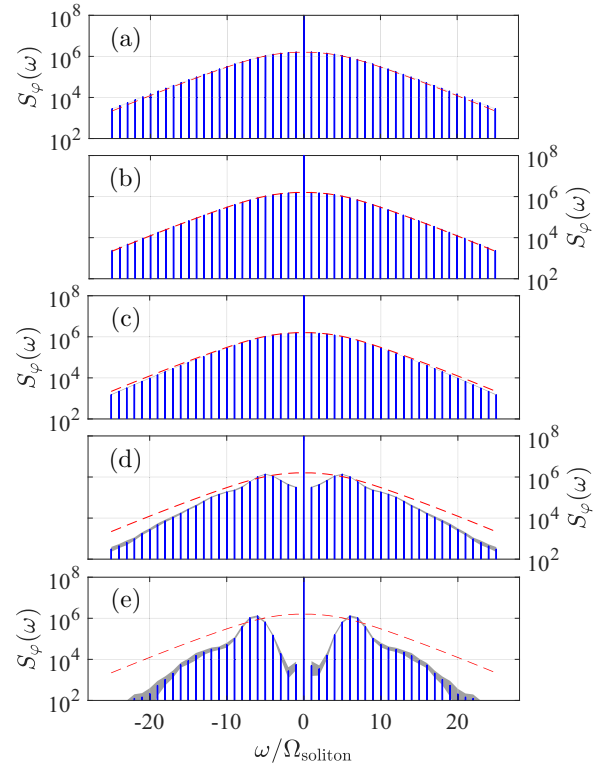


FIG. 9. Fourier spectrum obtained by considering 51 modes for (a)  $\tilde{N} = 1$ , (b)  $\tilde{N} = 4 \times 10^{-4}$ , (c)  $\tilde{N} = 10^{-4}$ , (d)  $\tilde{N} = 2.5 \times 10^{-5}$ , and (e)  $\tilde{N} = 1.1 \times 10^{-5}$ . The gray region shows the 95% standard deviation. The red dashed lines represent the envelope of the Fourier spectrum obtained from the GPE.

where quantum effects produce a significant departure from the predictions of the classical GP equation.

## IV. CONCLUSIONS

We have carried out a theoretical study of DKSs in microring resonators in terms of the truncated Wigner approximation, which describes quantum fluctuations to leading order in  $\hbar$  and is therefore well suited for the description of regimes of large photon occupation as in current experiments. We have shown that quantum effects are responsible for a finite coherence time of the soliton, which in the long-time limit leaves room for an average solution with the field uniformly distributed along the ring. The timescale of the soliton decay towards the steady-state solution depends on the relative size of quantum fluctuations and decreases when quantum fluctuations become larger. A scaling analysis of the TWA equations indicates that a regime with large quantum effects may be achieved by decreasing the driving-field intensity while correspondingly increasing the strength of the Kerr nonlinearity. The analysis provides clear indications about whether this behavior can be observed in experiments.

We have additionally shown that the timescale associated with the soliton disappearance is determined by the inverse Liouvillian spectral gap. More precisely, by studying the power spectrum of the DKS, we have inferred the complex eigenvalues of the Liouvillian superoperator which governs

the dynamics of the DKS as an open quantum system. We have shown that the eigenvalues with the largest real part—besides the zero-eigenvalue associated with the spatially uniform steady state—are arranged to have a constant (negative) real part, defining the Liouvillian gap, and evenly spaced imaginary parts, corresponding to the Kerr frequency comb. This arrangement emerges asymptotically in the limit of large input power, and the Liouvillian gap vanishes as a power law of the total photon occupation in the microring modes. We have therefore shown that DKSs are a specific manifestation of a dissipative time crystal—a general phenomenon which can arise in open quantum systems and has

been extensively studied in recent times. Establishing the link between DKSs and dissipative time crystals is an important step in the study and characterization of spontaneous time-translational symmetry breaking in quantum systems out of equilibrium.

#### ACKNOWLEDGMENTS

We acknowledge enlightening discussions with J. P. Vasco. This work was supported by the Swiss National Science Foundation through Projects No. 200021\_162357 and No. 200020\_185015.

- 
- [1] Y. K. Chembo, Kerr optical frequency combs: Theory, applications and perspectives, *Nanophotonics* **5**, 214 (2016).
- [2] M. Kues, C. Reimer, J. M. Lukens, W. J. Munro, A. M. Weiner, D. J. Moss, and R. Morandotti, Quantum optical microcombs, *Nat. Photonics* **13**, 170 (2019).
- [3] M. Karpov, M. H. P. Pfeiffer, H. Guo, W. Weng, J. Liu, and T. J. Kippenberg, Dynamics of soliton crystals in optical microresonators, *Nat. Phys.* **15**, 1071 (2019).
- [4] A. Kovach, D. Chen, J. He, H. Choi, A. H. Dogan, M. Ghasemkhani, H. Taheri, and A. M. Armani, Emerging material systems for integrated optical Kerr frequency combs, *Adv. Opt. Photonics* **12**, 135 (2020).
- [5] S. A. Diddams, K. Vahala, and T. Udem, Optical frequency combs: Coherently uniting the electromagnetic spectrum, *Science* **369**, eaay3676 (2020).
- [6] T. J. Kippenberg, A. L. Gaeta, M. Lipson, and M. L. Gorodetsky, Dissipative Kerr solitons in optical microresonators, *Science* **361**, eaan8083 (2018).
- [7] P. Del’Haye, A. Schliesser, O. Arcizet, T. Wilken, R. Holzwarth, and T. J. Kippenberg, Optical frequency comb generation from a monolithic microresonator, *Nature (London)* **450**, 1214 (2007).
- [8] T. J. Kippenberg, R. Holzwarth, and S. A. Diddams, Microresonator-based optical frequency combs, *Science* **332**, 555 (2011).
- [9] T. Udem, R. Holzwarth, and T. W. Hänsch, Optical frequency metrology, *Nature (London)* **416**, 233 (2002).
- [10] A. L. Gaeta, M. Lipson, and T. J. Kippenberg, Photonic-chip-based frequency combs, *Nat. Photonics* **13**, 158 (2019).
- [11] X. Yi, Q.-F. Yang, K. Y. Yang, M.-G. Suh, and K. Vahala, Soliton frequency comb at microwave rates in a high-Q silica microresonator, *Optica* **2**, 1078 (2015).
- [12] J. Ma, L. Xiao, J. Gu, H. Li, X. Cheng, G. He, X. Jiang, and M. Xiao, Visible Kerr comb generation in a high-Q silica microdisk resonator with a large wedge angle, *Photonics Res.* **7**, 573 (2019).
- [13] A. A. Savchenkov, A. B. Matsko, V. S. Ilchenko, I. Solomatine, D. Seidel, and L. Maleki, Tunable Optical Frequency Comb with a Crystalline Whispering Gallery Mode Resonator, *Phys. Rev. Lett.* **101**, 093902 (2008).
- [14] J. S. Levy, A. Gondarenko, M. A. Foster, A. C. Turner-Foster, A. L. Gaeta, and M. Lipson, CMOS-compatible multiple-wavelength oscillator for on-chip optical interconnects, *Nat. Photonics* **4**, 37 (2010).
- [15] F. Ferdous, H. Miao, D. E. Leaird, K. Srinivasan, J. Wang, L. Chen, L. T. Varghese, and A. M. Weiner, Spectral line-by-line pulse shaping of on-chip microresonator frequency combs, *Nat. Photonics* **5**, 770 (2011).
- [16] Y. Okawachi, K. Saha, J. S. Levy, Y. H. Wen, M. Lipson, and A. L. Gaeta, Octave-spanning frequency comb generation in a silicon nitride chip, *Opt. Lett.* **36**, 3398 (2011).
- [17] C. Joshi, J. K. Jang, K. Luke, X. Ji, S. A. Miller, A. Klenner, Y. Okawachi, M. Lipson, and A. L. Gaeta, Thermally controlled comb generation and soliton modelocking in microresonators, *Opt. Lett.* **41**, 2565 (2016).
- [18] V. Brasch, M. Geiselmann, T. Herr, G. Lihachev, M. H. P. Pfeiffer, M. L. Gorodetsky, and T. J. Kippenberg, Photonic chip-based optical frequency comb using soliton Cherenkov radiation, *Science* **351**, 357 (2016).
- [19] B. J. M. Hausmann, I. Bulu, V. Venkataraman, P. Deotare, and M. Lončar, Diamond nonlinear photonics, *Nat. Photonics* **8**, 369 (2014).
- [20] H. Jung, C. Xiong, K. Y. Fong, X. Zhang, and H. X. Tang, Optical frequency comb generation from aluminum nitride microring resonator, *Opt. Lett.* **38**, 2810 (2013).
- [21] H. Jung, R. Stoll, X. Guo, D. Fischer, and H. X. Tang, Green, red, and IR frequency comb line generation from single IR pump in AlN microring resonator, *Optica* **1**, 396 (2014).
- [22] Y. He, Q.-F. Yang, J. Ling, R. Luo, H. Liang, M. Li, B. Shen, H. Wang, K. Vahala, and Q. Lin, Self-starting bi-chromatic LiNbO<sub>3</sub> soliton microcomb, *Optica* **6**, 1138 (2019).
- [23] C. Wang, M. Zhang, M. Yu, R. Zhu, H. Hu, and M. Loncar, Monolithic lithium niobate photonic circuits for Kerr frequency comb generation and modulation, *Nat. Commun.* **10**, 978 (2019).
- [24] A. G. Griffith, R. K. Lau, J. Cardenas, Y. Okawachi, A. Mohanty, R. Fain, Y. H. D. Lee, M. Yu, C. T. Phare, C. B. Poitras, A. L. Gaeta, and M. Lipson, Silicon-chip mid-infrared frequency comb generation, *Nat. Commun.* **6**, 6299 (2015).
- [25] F. Leo, S. Coen, P. Kockaert, S.-P. Gorza, P. Emplit, and M. Haelterman, Temporal cavity solitons in one-dimensional Kerr media as bits in an all-optical buffer, *Nat. Photonics* **4**, 471 (2010).
- [26] T. Herr, V. Brasch, J. D. Jost, C. Y. Wang, N. M. Kondratiev, M. L. Gorodetsky, and T. J. Kippenberg, Temporal solitons in optical microresonators, *Nat. Photonics* **8**, 145 (2014).
- [27] A. M. Weiner, Cavity solitons come of age, *Nat. Photonics* **11**, 533 (2017).

- [28] M. Karpov, Dynamics and applications of dissipative Kerr solitons, Ph.D. thesis, EPFL, Lausanne, 2020.
- [29] V. E. Lobanov, A. E. Shitikov, R. R. Galiev, K. N. Min'kov, and N. M. Kondratiev, Generation and properties of dissipative Kerr solitons and platicons in optical microresonators with backscattering, *Opt. Express* **28**, 36544 (2020).
- [30] P. Grelu, *Nonlinear Optical Cavity Dynamics: From Microresonators to Fiber Lasers* (Wiley-VCH, Weinheim, 2016).
- [31] L. Lugiato, *Nonlinear Optical Systems* (Cambridge University Press, Cambridge, 2015).
- [32] S. B. Papp, K. Beha, P. Del'Haye, F. Quinlan, H. Lee, K. J. Vahala, and S. A. Diddams, Microresonator frequency comb optical clock, *Optica* **1**, 10 (2014).
- [33] V. Gerginov, C. E. Tanner, S. A. Diddams, A. Bartels and L. Hollberg, High-resolution spectroscopy with a femtosecond laser frequency comb, *Opt. Lett.* **30**, 1734 (2005).
- [34] S. B. Papp, P. Del'Haye, and S. A. Diddams, Mechanical Control of a Microrod-Resonator Optical Frequency Comb, *Phys. Rev. X* **3**, 031003 (2013).
- [35] P. Del'Haye, O. Arcizet, A. Schliesser, R. Holzwarth, and T. J. Kippenberg, Full Stabilization of a Microresonator-Based Optical Frequency Comb, *Phys. Rev. Lett.* **101**, 053903 (2008).
- [36] P. Del'Haye, S. B. Papp and S. A. Diddams, Hybrid Electro-optically Modulated Microcombs, *Phys. Rev. Lett.* **109**, 263901 (2012).
- [37] D. T. Spencer *et al.*, An optical-frequency synthesizer using integrated photonics, *Nature (London)* **557**, 81 (2018).
- [38] J. Pfeifle, V. Brasch, M. Lauermann, Y. Yu, D. Wegner, T. Herr, K. Hartinger, P. Schindler, J. Li, D. Hillerkuss, R. Schmogrow, C. Weimann, R. Holzwarth, W. Freude, J. Leuthold, T. J. Kippenberg, and C. Koos, Coherent terabit communications with microresonator Kerr frequency combs, *Nat. Photonics* **8**, 375 (2014).
- [39] J. Pfeifle, A. Coillet, R. Henriët, K. Saleh, P. Schindler, C. Weimann, W. Freude, I. V. Balakireva, L. Larger, C. Koos, and Y. K. Chembo, Optimally Coherent Kerr Combs Generated with Crystalline Whispering Gallery Mode Resonators for Ultrahigh Capacity Fiber Communications, *Phys. Rev. Lett.* **114**, 093902 (2015).
- [40] P. Marin-Palomo, J. N. Kemal, M. Karpov, A. Kordts, J. Pfeifle, M. H. P. Pfeiffer, P. Trocha, S. Wolf, V. Brasch, M. H. Anderson, R. Rosenberger, K. Vijayan, W. Freude, T. J. Kippenberg, and C. Koos, Microresonator-based solitons for massively parallel coherent optical communications, *Nature (London)* **546**, 274 (2017).
- [41] B. Bernhardt, A. Ozawa, P. Jacquet, M. Jacquy, Y. Kobayashi, T. Udem, R. Holzwarth, G. Guelachvili, T. W. Hänsch, and N. Picqué, Cavity-enhanced dual-comb spectroscopy, *Nat. Photonics* **4**, 55 (2010).
- [42] M. Yu, Y. Okawachi, C. Joshi, X. Ji, M. Lipson, and A. L. Gaeta, Gas-Phase Microresonator-Based Comb Spectroscopy without an External Pump Laser, *ACS Photonics* **5**, 2780 (2018).
- [43] M. C. Stowe, F. C. Cruz, A. Marian, and J. Ye, High Resolution Atomic Coherent Control via Spectral Phase Manipulation of an Optical Frequency Comb, *Phys. Rev. Lett.* **96**, 153001 (2006).
- [44] D. C. Heinecke, A. Bartels, T. M. Fortier, D. A. Braje, L. Hollberg, and S. A. Diddams, Optical frequency stabilization of a 10 GHz Ti:sapphire frequency comb by saturated absorption spectroscopy in  $^{87}$ rubidium, *Phys. Rev. A* **80**, 053806 (2009).
- [45] I. Barmes, S. Witte, and K. S. E. Eikema, High-Precision Spectroscopy with Counterpropagating Femtosecond Pulses, *Phys. Rev. Lett.* **111**, 023007 (2013).
- [46] J. Morgenweg, I. Barmes, and K. S. E. Eikema, Ramsey-comb spectroscopy with intense ultrashort laser pulses, *Nat. Phys.* **10**, 30 (2014).
- [47] A. Cingöz, D. C. Yost, T. K. Allison, A. Ruehl, M. E. Fermann, I. Hartl, and J. Ye, Direct frequency comb spectroscopy in the extreme ultraviolet, *Nature (London)* **482**, 68 (2012).
- [48] M.-G. Suh, Q.-F. Yang, K. Y. Yang, X. Yi, and K. J. Vahala, Microresonator soliton dual-comb spectroscopy, *Science* **354**, 600 (2016).
- [49] C. Reimer, M. Kues, P. Roztocky, B. Wetzel, F. Grazioso, B. E. Little, S. T. Chu, T. Johnston, Y. Bromberg, L. Caspani, D. J. Moss, and R. Morandotti, Generation of multiphoton entangled quantum states by means of integrated frequency combs, *Science* **351**, 1176 (2016).
- [50] M. Pysker, Y. Miwa, R. Shahrokhshahi, R. Bloomer, and O. Pfister, Parallel Generation of Quadripartite Cluster Entanglement in the Optical Frequency Comb, *Phys. Rev. Lett.* **107**, 030505 (2011).
- [51] J. Roslund, R. M. de Araújo, S. Jiang, C. Fabre, and N. Treps, Wavelength-multiplexed quantum networks with ultrafast frequency combs, *Nat. Photonics* **8**, 109 (2014).
- [52] M. Chen, N. C. Menicucci, and O. Pfister, Experimental Realization of Multipartite Entanglement of 60 Modes of a Quantum Optical Frequency Comb, *Phys. Rev. Lett.* **112**, 120505 (2014).
- [53] M. Kues, C. Reimer, P. Roztocky, L. R. Cortés, S. Sciara, B. Wetzel, Y. Zhang, A. Cino, S. T. Chu, B. E. Little, D. J. Moss, L. Caspani, J. Azaña, and R. Morandotti, On-chip generation of high-dimensional entangled quantum states and their coherent control, *Nature (London)* **546**, 622 (2017).
- [54] P. Imany, J. A. Jaramillo-Villegas, O. D. Odele, K. Han, D. E. Leaird, J. M. Lukens, P. Lougovski, M. Qi, and A. M. Weiner, 50-GHz-spaced comb of high-dimensional frequency-bin entangled photons from an on-chip silicon nitride microresonator, *Opt. Express* **26**, 1825 (2018).
- [55] Z. Yang, M. Jahanbozorgi, D. Jeong, S. Sun, O. Pfister, H. Lee, and X. Yi, A squeezed quantum microcomb on a chip, *Nat. Commun.* **12**, 4781 (2021).
- [56] M. A. Guidry, D. M. Lukin, K. Y. Yang, R. Trivedi, and J. Vučković, Quantum optics of soliton microcombs *Nature Photonics* **16**, 52 (2022).
- [57] Y. K. Chembo, Quantum dynamics of Kerr optical frequency combs below and above threshold: Spontaneous four-wave mixing, entanglement, and squeezed states of light, *Phys. Rev. A* **93**, 033820 (2016).
- [58] C. Gardiner and P. Zoller, *Quantum Noise: A Handbook of Markovian and Non-Markovian Quantum Stochastic Methods with Applications to Quantum Optics*, Springer Series in Synergetics (Springer, Berlin, Heidelberg, 2000).
- [59] D. Walls and G. Milburn, *Quantum Optics* (Springer, Berlin, 2008).
- [60] K. Vogel and H. Risken, Quasiprobability distributions in dispersive optical bistability, *Phys. Rev. A* **39**, 4675 (1989).

- [61] B. Opanchuk and P. D. Drummond, Functional Wigner representation of quantum dynamics of Bose-Einstein condensate, *J. Math. Phys.* **54**, 042107 (2013).
- [62] P. D. Drummond and B. Opanchuk, Truncated Wigner dynamics and conservation laws, *Phys. Rev. A* **96**, 043616 (2017).
- [63] A. Polkovnikov, Phase space representation of quantum dynamics, *Ann. Phys. (NY)* **325**, 1790 (2010).
- [64] V. V. Albert and L. Jiang, Symmetries and conserved quantities in Lindblad master equations, *Phys. Rev. A* **89**, 022118 (2014).
- [65] D. Nigro, On the uniqueness of the steady-state solution of the Lindblad–Gorini–Kossakowski–Sudarshan equation, *J. Stat. Mech.* (2019) 043202.
- [66] F. Minganti, A. Biella, N. Bartolo, and C. Ciuti, Spectral theory of Liouvillians for dissipative phase transitions, *Phys. Rev. A* **98**, 042118 (2018).
- [67] F. Iemini, A. Russomanno, J. Keeling, M. Schirò, M. Dalmonte, and R. Fazio, Boundary Time Crystals, *Phys. Rev. Lett.* **121**, 035301 (2018).
- [68] J. Zhang, P. W. Hess, A. Kyprianidis, P. Becker, A. Lee, J. Smith, G. Pagano, I.-D. Potirniche, A. C. Potter, A. Vishwanath, N. Y. Yao, and C. Monroe, Observation of a discrete time crystal, *Nature (London)* **543**, 217 (2017).
- [69] H. Taheri, A. B. Matsko, L. Maleki, and K. Sacha, All-optical dissipative discrete time crystals, *Nat. Commun.* **13**, 848 (2022).
- [70] K. Sacha and J. Zakrzewski, Time crystals: A review, *Rep. Prog. Phys.* **81**, 016401 (2018).
- [71] K. Nakatsugawa, T. Fujii, and S. Tanda, Quantum time crystal by decoherence: Proposal with an incommensurate charge density wave ring, *Phys. Rev. B* **96**, 094308 (2017).
- [72] R. R. W. Wang, B. Xing, G. G. Carlo, and D. Poletti, Period doubling in period-one steady states, *Phys. Rev. E* **97**, 020202 (2018).
- [73] K. Tucker, B. Zhu, R. J. Lewis-Swan, J. Marino, F. Jimenez, J. G. Restrepo, and A. M. Rey, Shattered time: Can a dissipative time crystal survive many-body correlations?, *New J. Phys.* **20**, 123003 (2018).
- [74] Z. Gong, R. Hamazaki, and M. Ueda, Discrete Time-Crystalline Order in Cavity and Circuit QED Systems, *Phys. Rev. Lett.* **120**, 040404 (2018).
- [75] E. T. Owen, J. Jin, D. Rossini, R. Fazio, and M. J. Hartmann, Quantum correlations and limit cycles in the driven-dissipative Heisenberg lattice, *New J. Phys.* **20**, 045004 (2018).
- [76] C. Lledó, T. K. Mavrogordatos, and M. H. Szymańska, Driven Bose-Hubbard dimer under nonlocal dissipation: A bistable time crystal, *Phys. Rev. B* **100**, 054303 (2019).
- [77] J. O’Sullivan, O. Lunt, C. W. Zollitsch, M. L. W. Thewalt, J. J. L. Morton, and A. Pal, Dissipative discrete time crystals, *arXiv:1807.09884* (2018).
- [78] F. M. Gambetta, F. Carollo, M. Marcuzzi, J. P. Garrahan, and I. Lesanovsky, Discrete Time Crystals in the Absence of Manifest Symmetries or Disorder in Open Quantum Systems, *Phys. Rev. Lett.* **122**, 015701 (2019).
- [79] A. V. Nalitov, H. Sigurdsson, S. Morina, Y. S. Krivosenko, I. V. Iorsh, Y. G. Rubo, A. V. Kavokin, and I. A. Shelykh, Optically trapped polariton condensates as semiclassical time crystals, *Phys. Rev. A* **99**, 033830 (2019).
- [80] H. Keßler, J. G. Cosme, M. Hemmerling, L. Mathey, and A. Hemmerich, Emergent limit cycles and time crystal dynamics in an atom-cavity system, *Phys. Rev. A* **99**, 053605 (2019).
- [81] B. Zhu, J. Marino, N. Y. Yao, M. D. Lukin, and E. A. Demler, Dicke time crystals in driven-dissipative quantum many-body systems, *New J. Phys.* **21**, 073028 (2019).
- [82] N. Dogra, M. Landini, K. Kroeger, L. Hruby, T. Donner, and T. Esslinger, Dissipation-induced structural instability and chiral dynamics in a quantum gas, *Science* **366**, 1496 (2019).
- [83] E. I. R. Chiacchio and A. Nunnenkamp, Dissipation-Induced Instabilities of a Spinor Bose-Einstein Condensate Inside an Optical Cavity, *Phys. Rev. Lett.* **122**, 193605 (2019).
- [84] B. Buča and D. Jaksch, Dissipation Induced Nonstationarity in a Quantum Gas, *Phys. Rev. Lett.* **123**, 260401 (2019).
- [85] B. Buča, J. Tindall, and D. Jaksch, Non-stationary coherent quantum many-body dynamics through dissipation, *Nat. Commun.* **10**, 1730 (2019).
- [86] C. Lledó and M. H. Szymańska, A dissipative time crystal with or without Z2 symmetry breaking, *New J. Phys.* **22**, 075002 (2020).
- [87] A. Lazarides, S. Roy, F. Piazza, and R. Moessner, Time crystallinity in dissipative Floquet systems, *Phys. Rev. Research* **2**, 022002 (2020).
- [88] K. Chinzei and T. N. Ikeda, Time Crystals Protected by Floquet Dynamical Symmetry in Hubbard Models, *Phys. Rev. Lett.* **125**, 060601 (2020).
- [89] H. Keßler, J. G. Cosme, C. Georges, L. Mathey, and A. Hemmerich, From a continuous to a discrete time crystal in a dissipative atom-cavity system, *New J. Phys.* **22**, 085002 (2020).
- [90] C. Booker, B. Buča and D. Jaksch, Non-stationarity and dissipative time crystals: Spectral properties and finite-size effects, *New J. Phys.* **22**, 085007 (2020).
- [91] G. Engelhardt and J. Cao, Dynamical Symmetries and Symmetry-Protected Selection Rules in Periodically Driven Quantum Systems, *Phys. Rev. Lett.* **126**, 090601 (2021).
- [92] D. Barberena, R. J. Lewis-Swan, J. K. Thompson, and A. M. Rey, Driven-dissipative quantum dynamics in ultra-long-lived dipoles in an optical cavity, *Phys. Rev. A* **99**, 053411 (2019).
- [93] J. G. Cosme, J. Skulte, and L. Mathey, Time crystals in a shaken atom-cavity system, *Phys. Rev. A* **100**, 053615 (2019).
- [94] J. Tindall, B. Buča, J. R. Coulthard, and D. Jaksch, Heating-Induced Long-Range  $\eta$  Pairing in the Hubbard Model, *Phys. Rev. Lett.* **123**, 030603 (2019).
- [95] K. Seibold, R. Rota, and V. Savona, Dissipative time crystal in an asymmetric nonlinear photonic dimer, *Phys. Rev. A* **101**, 033839 (2020).
- [96] R. Hurtado-Gutiérrez, F. Carollo, C. Pérez-Espigares, and P. I. Hurtado, Building Continuous Time Crystals from Rare Events, *Phys. Rev. Lett.* **125**, 160601 (2020).
- [97] L. F. d. Prazeres, L. d. S. Souza, and F. Iemini, Boundary time crystals in collective  $d$ -level systems, *Phys. Rev. B* **103**, 184308 (2021).
- [98] F. Minganti, I. I. Arkhipov, A. Miranowicz, and F. Nori, Correspondence between dissipative phase transitions of light and time crystals, *arXiv:2008.08075* (2020).
- [99] H. Keßler, P. Kongkhambut, C. Georges, L. Mathey, J. G. Cosme, and A. Hemmerich, Observation of a Dissipative Time Crystal, *Phys. Rev. Lett.* **127**, 043602 (2021).
- [100] D. A. Lidar, Lecture notes on the theory of open quantum systems, *arXiv:1902.00967*.
- [101] V. V. Albert, B. Bradlyn, M. Fraas, and L. Jiang, Geometry and Response of Lindbladians, *Phys. Rev. X* **6**, 041031 (2016).

- [102] B. Baumgartner and H. Narnhofer, Analysis of quantum semi-groups with GKS–Lindblad generators: II. General, *J. Phys. A* **41**, 395303 (2008).
- [103] P. E. Barclay, K. Srinivasan, and O. Painter, Nonlinear response of silicon photonic crystal microresonators excited via an integrated waveguide and fiber taper, *Opt. Express* **13**, 801 (2005).
- [104] J. Vasco and V. Savona, Slow-Light Frequency Combs and Dissipative Kerr Solitons in Coupled-Cavity Waveguides, *Phys. Rev. Appl.* **12**, 064065 (2019).
- [105] H.-P. Breuer, *The Theory of Open Quantum Systems* (Clarendon, Oxford, 2007).
- [106] L. A. Lugiato and R. Lefever, Spatial Dissipative Structures in Passive Optical Systems, *Phys. Rev. Lett.* **58**, 2209 (1987).
- [107] C. Godey, I. V. Balakireva, A. Coillet, and Y. K. Chembo, Stability analysis of the spatiotemporal Lugiato-Lefever model for Kerr optical frequency combs in the anomalous and normal dispersion regimes, *Phys. Rev. A* **89**, 063814 (2014).
- [108] C. W. Gardiner, *Handbook of Stochastic Methods for Physics, Chemistry, and the Natural Sciences* (Springer, Berlin, 1985).
- [109] K. E. Cahill and R. J. Glauber, Density Operators and Quasiprobability Distributions, *Phys. Rev.* **177**, 1882 (1969).
- [110] X. Ji, F. A. S. Barbosa, S. P. Roberts, A. Dutt, J. Cardenas, Y. Okawachi, A. Bryant, A. L. Gaeta, and M. Lipson, Ultra-low-loss on-chip resonators with sub-milliwatt parametric oscillation threshold, *Optica* **4**, 619 (2017).
- [111] K. Liu, S. Yao, and C. Yang, Raman pure quartic solitons in Kerr microresonators, *Opt. Lett.* **46**, 993 (2021).
- [112] K. Ikeda, R. E. Saperstein, N. Alic, and Y. Fainman, Thermal and Kerr nonlinear properties of plasma-deposited silicon nitride/silicon dioxide waveguides, *Opt. Express* **16**, 12987 (2008).
- [113] F. Vicentini, F. Minganti, R. Rota, G. Orso, and C. Ciuti, Critical slowing down in driven-dissipative Bose-Hubbard lattices, *Phys. Rev. A* **97**, 013853 (2018).